Investigation of interface states in single-negative metamaterial layered structures based on the phase properties

Jian Zheng,[1] Yihang Chen,[1,3,*] Zefeng Chen,[1,2] Xinggang Wang,[1] Peng Han,[1] Zehui Yong,[2] Yu Wang,[2] Chi Wah Leung,[2,4] and Costas M. Soukoulis[3]

[1]*Laboratory of Quantum Information Technology, School of Physics and Telecommunication Engineering, South China Normal University, Guangzhou 510006, China*

[2]*Department of Applied Physics and Materials Research Center, The Hong Kong Polytechnic University, Hong Kong SAR, China*

[3]*Ames Laboratory and Department of Physics and Astronomy, Iowa State University, Ames, Iowa 50011, USA*

[4]*dennis.leung@polyu.edu.hk*

[*]*chenyh@ameslab.gov*

Abstract: The physical mechanism of the interface states in layered structures consisting of single-negative metamaterials is investigated using a simple resonant cavity model. We found that the interface states and their corresponding tunneling transmission modes appeared when the resonant condition is satisfied. Such resonant condition depends on the phase changes inside the resonant cavity. Based on these results, we proposed an efficient method to precisely predict the frequencies of the tunneling interface states inside the single-negative metamaterial layers. Our method is effective for interface states corresponding to perfect or imperfect tunneling transmission. Composite right/left-handed transmission lines were used to realize the pair and sandwich metamaterial layered structures in the microwave region. Electromagnetic tunneling interface states were observed in the measurements, which agreed well with the theory. Our study offers a way for effectively designing metamaterial devices with novel electromagnetic tunneling properties.

OCIS codes: (260.2110) Electromagnetic optics; (160.3918) Metamaterials; (350.5030) Phase.

References and links

1. S. Kawata, Y. Inouye, and P. Verma, "Plasmonics for near-field nano-imaging and superlensing," Nat. Photonics **3**(7), 388–394 (2009).
2. A. V. Krasavin, A. V. Zayats, and N. I. Zheludev, "Active control of surface plasmon-polariton waves," J. Opt. A, Pure Appl. Opt. **7**(2), S85–S89 (2005).
3. O. Gazzano, S. M. de Vasconcellos, K. Gauthron, C. Symonds, J. Bloch, P. Voisin, J. Bellessa, A. Lemaître, and P. Senellart, "Evidence for confined Tamm plasmon modes under metallic microdisks and application to the control of spontaneous optical emission," Phys. Rev. Lett. **107**(24), 247402 (2011).
4. A. Kavokin, I. Shelykh, and G. Malpuech, "Optical Tamm states for the fabrication of polariton lasers," Appl. Phys. Lett. **87**(26), 261105 (2005).
5. W. L. Barnes, A. Dereux, and T. W. Ebbesen, "Surface plasmon subwavelength optics," Nature **424**(6950), 824–830 (2003).
6. J. Homola, S. S. Yee, and G. Gauglitz, "Surface plasmon resonance sensors: review," Sens. Actuators B Chem. **54**(1-2), 3–15 (1999).
7. K. Kneipp, H. Kneipp, I. Itzkan, R. R. Dasari, and M. S. Feld, "Surface-enhanced Raman scattering and biophysics," J. Phys. Condens. Matter **14**(18), R597–R624 (2002).
8. A. V. Kavokin, I. A. Shelykh, and G. Malpuech, "Lossless interface modes at the boundary between two periodic dielectric structures," Phys. Rev. B **72**(23), 233102 (2005).
9. H. Shin and S. Fan, "All-angle negative refraction for surface plasmon waves using a metal-dielectric-metal structure," Phys. Rev. Lett. **96**(7), 073907 (2006).
10. T. Goto, A. V. Dorofeenko, A. M. Merzlikin, A. V. Baryshev, A. P. Vinogradov, M. Inoue, A. A. Lisyansky, and A. B. Granovsky, "Optical Tamm states in one-dimensional magnetophotonic structures," Phys. Rev. Lett. **101**(11), 113902 (2008).
11. D. Ö. Güney, T. Koschny, and C. M. Soukoulis, "Surface plasmon driven electric and magnetic resonators for metamaterials," Phys. Rev. B **83**(4), 045107 (2011).

#188556 - $15.00 USD Received 10 Apr 2013; revised 7 Jun 2013; accepted 1 Jul 2013; published 5 Jul 2013

12. Z. F. Chen, P. Han, C. W. Leung, Y. Wang, M. Hu, and Y. Chen, "Study of optical Tamm states based on the phase properties of one-dimensional photonic crystals," Opt. Express **20**(19), 21618–21626 (2012).
13. A. V. Baryshev, K. Kawasaki, P. B. Lim, and M. Inoue, "Interplay of surface resonances in one-dimensional plasmonic magnetophotonic crystal slabs," Phys. Rev. B **85**(20), 205130 (2012).
14. A. Alù and N. Engheta, "Pairing an epsilon-negative slab with a mu-negative slab: resonance, tunneling and transparency," IEEE Trans. Antenn. Propag. **51**(10), 2558–2571 (2003).
15. D. K. Qing and G. Chen, "Enhancement of evanescent waves in waveguides using metamaterials of negative permittivity and permeability," Appl. Phys. Lett. **84**(5), 669–671 (2004).
16. T. Fujishige, C. Caloz, and T. Itoh, "Experimental demonstration of transparency in the ENG-MNG pair in a CRLH transmission line implementation," Microw. Opt. Technol. Lett. **46**(5), 476–481 (2005).
17. A. Alù, N. Engheta, and R. W. Ziolkowski, "Finite-difference time-domain analysis of the tunneling and growing exponential in a pair of ε-negative and μ-negative slabs," Phys. Rev. E Stat. Nonlin. Soft Matter Phys. **74**(1), 016604 (2006).
18. H. T. Jiang, H. Chen, H. Q. Li, Y. W. Zhang, J. Zi, and S. Y. Zhu, "Properties of one-dimensional photonic crystals containing single-negative materials," Phys. Rev. E Stat. Nonlin. Soft Matter Phys. **69**(6), 066607 (2004).
19. Y. H. Chen, J. W. Dong, and H. Z. Wang, "Twin defect modes in one-dimensional photonic crystals with a single-negative material defect," Appl. Phys. Lett. **89**(14), 141101 (2006).
20. R. P. Liu, B. Zhao, X. Q. Lin, Q. Cheng, and T. J. Cui, "Evanescent-wave amplification studied using a bilayer periodic circuit structure and its effective medium model," Phys. Rev. B **75**(12), 125118 (2007).
21. T. H. Feng, Y. H. Li, H. T. Jiang, Y. Sun, L. He, H. Q. Li, Y. W. Zhang, Y. L. Shi, and H. Chen, "Electromagnetic tunneling in a sandwich structure containing single negative media," Phys. Rev. E Stat. Nonlin. Soft Matter Phys. **79**(2), 026601 (2009).
22. A. Alù and N. Engheta, "Pairing an epsilon-negative slab with a mu-negative slab: resonance, tunneling and transparency," IEEE Trans. Microw. Theory Tech. **51**, 2558–2571 (2003).
23. D. R. Smith, J. B. Pendry, and M. C. K. Wiltshire, "Metamaterials and negative refractive index," Science **305**(5685), 788–792 (2004).
24. I. R. Hooper, T. W. Preist, and J. R. Sambles, "Making Tunnel Barriers (Including Metals) Transparent," Phys. Rev. Lett. **97**(5), 053902 (2006).
25. M. Born and E. Wolf, *Principles of Optics*, 7th (expanded) ed. (Cambridg University Press, Cambridge, 1999).
26. N. H. Liu, S. Y. Zhu, H. Chen, and X. Wu, "Superluminal pulse propagation through one-dimensional photonic crystals with a dispersive defect," Phys. Rev. E Stat. Nonlin. Soft Matter Phys. **65**(4 4 Pt 2B), 046607 (2002).
27. R. Ruppin, "Surface polaritons of a left-handed material slab," J. Phys. Condens. Matter **13**(9), 1811–1818 (2001).
28. E. Prodan, C. Radloff, N. J. Halas, and P. Nordlander, "A Hybridization Model for the Plasmon Response of Complex Nanostructures," Science **302**(5644), 419–422 (2003).
29. N. Liu, H. Liu, S. Zhu, and H. Giessen, "Stereometamaterials," Nat. Photonics **3**(3), 157–162 (2009).
30. J. B. Pendry, A. J. Holden, W. J. Stewart, and I. Youngs, "Extremely Low Frequency Plasmons in Metallic Mesostructures," Phys. Rev. Lett. **76**(25), 4773–4776 (1996).
31. R. A. Shelby, D. R. Smith, and S. Schultz, "Experimental Verification of a Negative Index of Refraction," Science **292**(5514), 77–79 (2001).
32. T. J. Yen, W. J. Padilla, N. Fang, D. C. Vier, D. R. Smith, J. B. Pendry, D. N. Basov, and X. Zhang, "Terahertz Magnetic Response from Artificial Materials," Science **303**(5663), 1494–1496 (2004).
33. G. V. Eleftheriades, A. K. Iyer, and P. C. Kremer, "Planar negative refractive index media using periodically *L*–*C* loaded transmission lines," IEEE Trans. Microw. Theory Tech. **50**(12), 2702–2712 (2002).
34. C. Caloz, A. Lai, and T. Itoh, "The challenge of homogenization in metamaterials," New J. Phys. **7**, 167 (2005).
35. I. Bahl, "Lumped Elements for RF and Microwave Circuits," (Artech House, 2003).

1. Introduction

Optical interface states, corresponding to the waves confined in the vicinity of the boundary between two optical media, have attracted much attention because of their far-ranging potential applications in near-field subwavelength imaging [1], optical switching [2], control of the optical emission [3], compact lasers [4], medicine and chemistry [5–7], etc. The properties of the optical interface states existing in different kinds of media, such as dielectrics, photonic crystals (PCs), and metals, have been widely studied [8–13]. Recently, the interface states were suggested to be present in metamaterial layers under certain conditions, which can lead to some novel features [14–22].

Metamaterials are artificial materials engineered to have ability to precisely control the dispersion and propagation of electromagnetic (EM) waves. Through variation of the subwavelength structural units, metamaterials allow for the tunability of permittivity ε and permeability μ that can span positive, negative, and near-zero values [23]. Therefore, single-negative (SNG) materials with specific negative value of ε or μ can be artificially realized. SNG metamaterials can be divided into two types, epsilon-negative (ENG) material whose ε

#188556 - $15.00 USD Received 10 Apr 2013; revised 7 Jun 2013; accepted 1 Jul 2013; published 5 Jul 2013

is negative, and mu-negative (MNG) material whose μ is negative. When several SNG metamaterials are brought together to form layered structures, special interface states with tunneling, localizing, and resonant enhancement phenomena may be observed [17–22]. Although some studies discussed the methods to determine when these interface states appear [21,22], they only mathematically focused on the complete tunneling cases with perfect transmission. Hence a more general theory to explain the appearance and the properties of the interface states in SNG metamaterial layers would be of interest.

In this paper, we study the physical mechanism of the interface states in SNG metamaterial layered structures using a resonant cavity model. According to such a model, an efficient way is proposed to precisely design the frequencies of the interface states using the phase changes inside the resonant cavity. Pair and sandwich SNG structures were fabricated and measured to verify our theory.

2. Model, theory and simulations

2.1 Resonant condition for SNG resonant cavity

Quantum mechanics brought forward the concept of particle tunneling that wave or particles may propagate through classically impenetrable barriers. Similar phenomena can be found in optics such as tunneling in the guise of frustrated total internal reflection, whereby evanescent optical fields penetrate across an air gap between two adjacent glass prisms, giving transmission of light beyond the critical angle for total internal reflection [24]. By drawing an analogy between optics and quantum mechanics (it can be considered although there is no exact equivalent to a potential for photons) [24], we consider a photonic well (by analogy to quantum well) formed by two opaque SNG metamaterial barriers, as shown in Fig. 1.

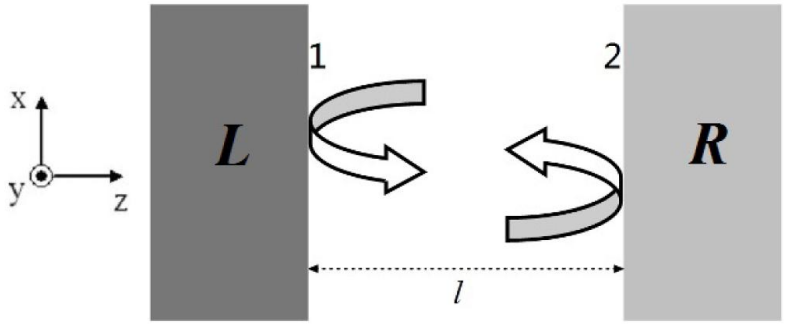

Fig. 1. A photonic well formed by two SNG metamaterials barriers.

Suppose the width of the well is *l*. After propagating through the well, a wave will gain a phase change $\varphi = nl\omega/c$, where n is the refractive index of the medium inside the well, ω is the angular frequency, c is the speed of electromagnetic wave in vacuum. We use $\varphi_1(\omega)$ and $\varphi_2(\omega)$ to represent the phase changes upon reflection from the left surface 1 and the right surface 2, respectively. In this case, the resonant condition of the structure can be written as

$$\varphi_1(\omega) + 2\varphi + \varphi_2(\omega) = 2m\pi, \tag{1}$$

where m is a integer. If the resonant condition is satisfied, a resonant enhancement will be observed, the EM wave can tunnel through the paired "photonic barriers" and an interface state forms. When the width of the photonic well decreases to be zero, φ becomes zero and Eq. (1) becomes

$$\varphi_1(\omega) + \varphi_2(\omega) = 2m\pi. \tag{2}$$

In this case, whether the interface state appears or not only depends on the values of $\varphi_1(\omega)$ and $\varphi_2(\omega)$. The phase changes can be calculated through the transfer matrix method [25]. The

#188556 - $15.00 USD Received 10 Apr 2013; revised 7 Jun 2013; accepted 1 Jul 2013; published 5 Jul 2013

transfer matrix for the left or right SNG barriers of the resonant cavity can be written in a form of

$$M_k = \begin{bmatrix} X_{11}^k & X_{12}^k \\ X_{21}^k & X_{22}^k \end{bmatrix}, \tag{3}$$

where $k = L$ or R. Consider a wave is incident from vacuum, we have the reflection coefficient [25,26]

$$r_k = |r_k| e^{i\varphi_k} = \frac{X_{22}^k - X_{11}^k + i(X_{12}^k + X_{21}^k)}{X_{22}^k + X_{11}^k + i(X_{12}^k - X_{21}^k)}. \tag{4}$$

The reflection phase changes can be obtained from Eq. (4). After getting the values of $\varphi_1(\omega)$ and $\varphi_2(\omega)$, one can obtains the number and the frequency positions of the tunneling interface modes. In the following sections, bi- and tri-layer SNG systems will be discussed.

2.2 Pair SNG layered system

We first consider a SNG bilayer system consisting of an ENG layer and a MNG layer with the thicknesses of 30 and 40 mm, respectively. Such a system can be regarded as a photonic well formed by sandwiching a zero thickness medium between an ENG barrier and a MNG barrier. We use a lossless Drude model to describe the dispersion of the metamaterials [18–21], that is

$$\varepsilon_{ENG} = 1 - \omega_{ep}^2 / \omega^2, \quad \mu_{ENG} = 3 \tag{5}$$

for ENG material layer, and

$$\varepsilon_{MNG} = 3, \mu_{MNG} = 1 - \omega_{mp}^2 / \omega^2 \tag{6}$$

for MNG material layer. ω_{ep} and ω_{mp} represent the electronic plasma frequencies and the magnetic plasma frequency, respectively. In this paper, our studies focus on the gigahertz range. Here we choose $\omega_{ep} = \omega_{mp} = 10$ GHz [18,19]. Figure 2(a) shows the transmittance and the phase changes as a function of frequency in the considered structure. In this case, the two metamaterial layers have a common SNG frequency range in about 0 ~1.60 GHz, within which they can both be seen as SNG material layers. As shown in Fig. 2, a tunneling transmission mode appears at 0.796 GHz. Such a transmission mode with the transmittance about 0.80 is not a perfect tunneling mode. It can also be seen from Fig. 2 that both $\varphi_1(\omega)$ and $\varphi_2(\omega)$ increase as the frequency increases. The value of $\varphi_1(\omega) + \varphi_2(\omega)$ equals zero at frequency 0.796 GHz, which means that the resonant condition of Eq. (2) is satisfied at frequency where the transmission mode exists. The electric field distribution corresponding to the transmission mode is also shown by the inset in Fig. 2. Strong field localization can be observed at the interface between ENG and MNG materials, which verifies that such a transmission mode is a surface plasmon mode. Therefore, from the resonant condition, one can obtain the frequency of the interface state of the SNG pair structure, even though the interface state does not correspond to a complete tunneling.

#188556 - $15.00 USD Received 10 Apr 2013; revised 7 Jun 2013; accepted 1 Jul 2013; published 5 Jul 2013

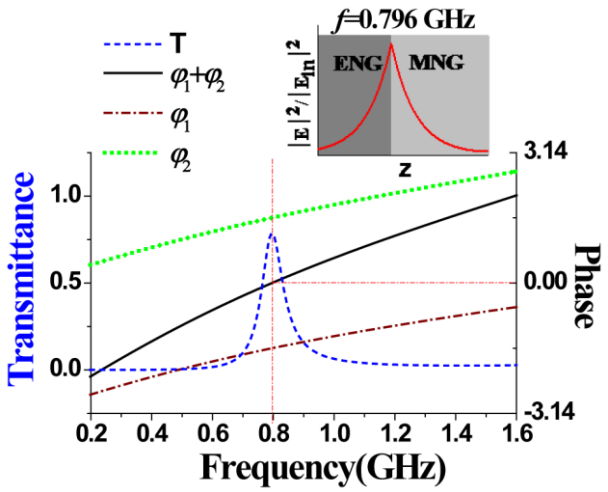

Fig. 2. Transmittance and phase changes as a function of frequency for pair SNG structures. The thicknesses of the ENG and MNG layers are 30 mm and 40 mm, respectively. The inset shows the electric field distribution at 0.796 GHz.

2.3 Sandwich SNG layered system

Next, we turn to the sandwich SNG structure. A symmetrical ENG-MNG-ENG layered structure is discussed first. Here, the considered system can be seen as possessing two barriers, the left ENG barrier and the right MNG-ENG barrier. In this section, we fix the thicknesses of the ENG layers as 30 mm. Figure 3 shows the transmission spectra and the phase change $\varphi_1(\omega) + \varphi_2(\omega)$ of the considered structure for different thickness of the MNG layer. As shown in Fig. 3(a), two tunneling transmission modes appear at 0.5305 GHz and 1.2066 GHz, where the resonant condition is satisfied since $\varphi_1(\omega) + \varphi_2(\omega) = 0$. The electric field distributions corresponding to the two tunneling modes are shown in the inset of Fig. 3(a), where the fields are mainly localized at the interfaces between the SNG materials. With the increase of d_{MNG}, the two interface states become closer and closer, and finally merge into each other as shown in Figs. 3(b)–3(d). It is noted that the resonance condition can certainly be satisfied at frequencies where the interface states appear.

The variation of the tunneling interface states shown in Fig. 3 can be understood as the result of the interaction of the surface plasmons. Surface plasmon polaritons may occur at interfaces where either permittivities or permeabilities of the two adjacent effective media have opposite signs [27]. Therefore, the interface between an ENG and a MNG material can support the surface plasmon resonance under certain condition. The considered ENG-MNG-ENG structure can be regarded as the cascade of two separate cavities, ENG-MNG and MNG-ENG. Since the sandwich structure is symmetrical, each of the ENG-MNG cavity and the MNG-ENG cavity supports the plasmon resonance at the same frequency. When these two cavities are placed together, the cavity plasmons interact with each other. This interaction results in the splitting of the original plasmon resonant mode into two new modes: the lower energy "bonding" plasmon and the higher energy "antibonding" plasmon [28,29]. The strength of the interaction of the cavity plasmons depends on the distance between the resonant cavities, i.e. the thickness of the MNG layer. As the thickness of the MNG layer increases, the plasmon interaction weakens, the frequency interval between the plasmon modes decreases. When the MNG layer is thick enough, the plasmons interaction is so weak that the two plasmon resonant modes become degenerate.

Similar tunneling interface states can be found in MNG-ENG-MNG structures. Such merging phenomena of the tunneling interface states may be used for designing double-channel filters. The frequencies and frequency interval of the transmission channels can be designed using the resonant condition based on the phase changes.

#188556 - $15.00 USD Received 10 Apr 2013; revised 7 Jun 2013; accepted 1 Jul 2013; published 5 Jul 2013

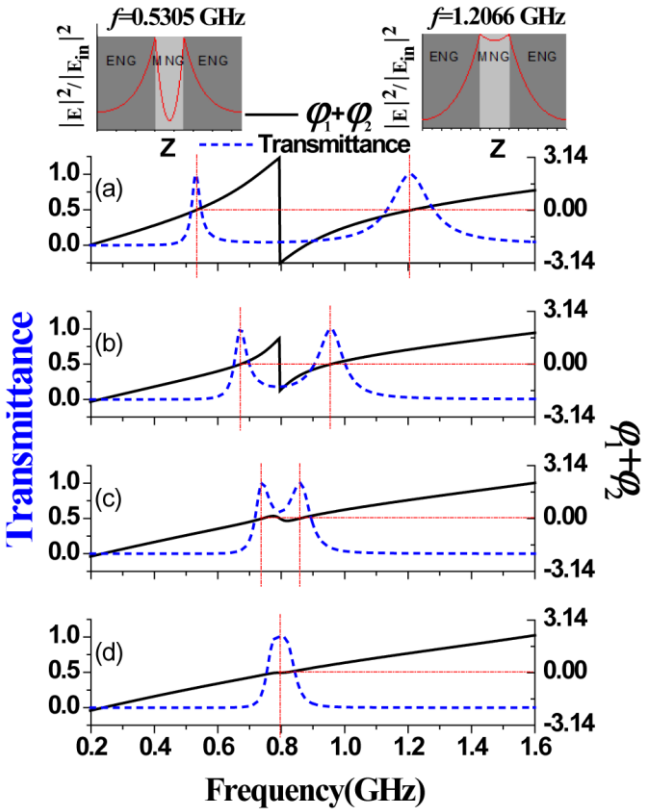

Fig. 3. Transmittance and phase change as a function of frequency for ENG-MNG-ENG sandwich structures, for different thicknesses of the MNG layer: (a) 15 mm, (b) 30 mm, (c) 45 mm, and (d) 60 mm.

3. Experiements and discussions

3.1 Design and fabrication for SNG metamaterials

Up to now, there are two main approaches to realize SNG metamaterials: resonant structures made of arrays of wires and split-ring resonators [30–32] and nonresonant transmission line (TL) structures made of lumped elements [16, 17, 33, 34]. The TL approach towards metamaterial with left-handed and right-handed attributes, known as composite right/left-handed transmission line (CRLH TL), presents the advantage of lower losses over a broader bandwidth. SNG material can be realized in the frequency range between the right-handed passband and left-handed passband of the CRLH TL. The CRLH TL is fabricated by the repetition of the TL unit cell, which consists of a host transmission line with lumped elements of series capacitors C and shunt inductors L [16, 33]. When the average lattice constant l_c is much smaller than the guided wavelength λ_g, the structure exhibits a macroscopic behavior which can be rigorously characterized in terms of the constitutive parameters ε and μ. In practice, $l_c < \lambda_g/4$ can be considered as the sufficient condition for the validity of homogeneous approximation [31]. In our experiment, 50Ω TL was used to fabricate CRLH TL which has FR-4 as substrates with thickness h = 1.6 mm and relative permittivity ε_{sub} = 4.75. The thickness of copper strip on the FR-4 substrate was t = 0.018 mm. The width of the copper strip was w = 2.945 mm corresponding to the characteristic impedance of Z_0 = 50.

For a one-dimensional CRLH TL, the constitutive parameters can be obtained by mapping the telegrapher's equations to Maxwell equations [33], the effective relative permittivity and permeability are given by the following approximate expressions

#188556 - $15.00 USD Received 10 Apr 2013; revised 7 Jun 2013; accepted 1 Jul 2013; published 5 Jul 2013

$$\varepsilon_j \approx \left(C_0 - 1/\omega^2 L_i d_i\right)/\left(\varepsilon_0 p\right), \quad \mu_j \approx p\left(L_0 - 1/\omega^2 C_i d_i\right)/\mu_0, \tag{7}$$

where C_0 and L_0 represent the distributed capacitance and inductance of the host TL, j represents the type of the CRLH TLs, and p is a structure constant which is given by $p = \sqrt{\mu_0/\left(\varepsilon_0 \varepsilon_{re}\right)}/Z_0$ [31]. For the microstrip lines considered here, the effective relative dielectric constant is ε_{re} = 3.556 [35]. As a result, we obtain p = 3.99, $C_0 = \sqrt{\varepsilon_{re}\varepsilon_0\mu_0}/Z_0 \approx 128$ pF/m, and $L_0 = Z_0^2 \times C_0 \approx 320$ nH/m.

SNG materials can be realized by CRLH TLs with suitable structural parameters. For examples, two types of CRLH TLs with 12 unit cells, A_{12} and B_{12}, were designed and fabricated. TL A_{12} possesses a unit length of l_A = 7.2 mm and loaded lumped elements C_A = 5.1 pF and L_A = 5.6 nH. TL B_{12} has a unit length of l_B = 8.4 mm and loaded lumped elements C_B = 2 pF and L_B = 10 nH.

The calculated relative permittivity ε_A and permeability μ_A of A_{12} are presented in Fig. 4(a). The simulated (by Advanced Design System (ADS)) and measured (by Agilent 8720ES *S*-parameter Network Analyzer) *S* parameters for A_{12} are shown in Fig. 4(b). S_{21} is the transmission coefficient through the transmission line. It is seen that both ε_A and μ_A are positive when the frequency is higher than 2.21 GHz, and a corresponding right-handed double-positive (DPS) passband exist in Fig. 4(b). On the other hand, both ε_A and μ_A are negative when the frequency is lower than 1.47 GHz and a corresponding left-handed double-negative (DNG) passband can be observed. In the frequency range 1.47 ~2.21 GHz, $\varepsilon_A < 0$ and $\mu_A > 0$, TL A_{12} is equivalent to an ENG material, a stopband appears since the wave number $k = 2\pi\sqrt{\varepsilon_1\mu_1}/\lambda_g$ is imaginary. As shown in Fig. 4(b), the measured result agrees with the simulations although inevitable losses led to a reduced transmittance. There is a cutoff frequency $f_i = 1/4\pi\sqrt{L_i C_i}$ for such high-pass CRLH TL [32]. It can be calculated that $f_A \approx 0.47$ GHz for TL A_{12}, and the propagation of EM wave is prohibited when the frequency is lower than this cutoff frequency, as shown in Fig. 4(b).

Similarly, the values of ε_B and μ_B, and the simulated and measured transmission spectra for TL B_{12} are shown in Figs. 4(c) and 4(d), respectively. It can be seen that a stop band corresponding to $\varepsilon_B > 0$ and $\mu_B < 0$ appears in the frequency range 1.53 ~2.17 GHz. TL B_{12} can be equivalent to a MNG material within such stop band. Consequently, both TLs A_{12} and B_{12} can be regarded as homogeneous SNG materials in frequencies between 1.53 and 2.17 GHz.

#188556 - $15.00 USD Received 10 Apr 2013; revised 7 Jun 2013; accepted 1 Jul 2013; published 5 Jul 2013

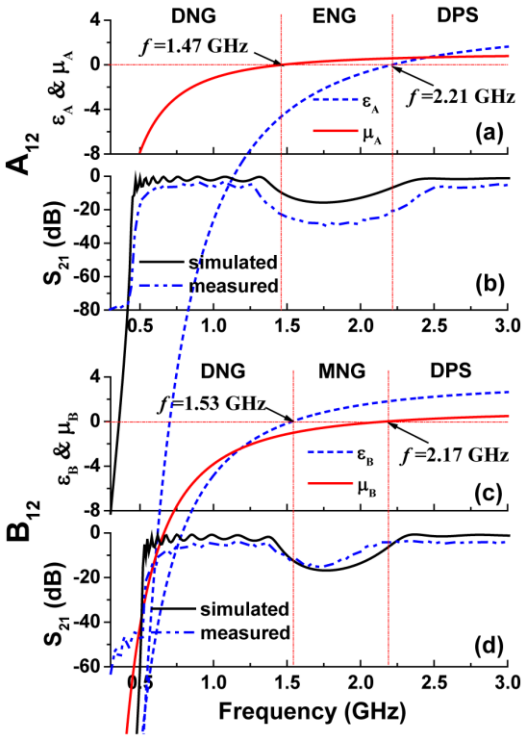

Fig. 4. Calculated effective permittivity and permeability, and the simulated and measured *S* parameters of the CRLH TLs A_{12} and B_{12}, respectively.

3.2 Experiment and simulations on the SNG pair system

Next, we investigated the properties of SNG pair structures using the CRLH TL structure. Figure 5 is the photograph of the fabricated A_6B_6 pair structure. The simulated and measured *S* parameters of this structure are shown in Fig. 6(a). The grey shaded areas represent the common SNG frequency region of both TLs *A* and *B*. Figure 6(b) shows the simulated value of $\varphi_1(\omega) + \varphi_2(\omega)$ as a function of frequency. As shown by the simulated results in Fig. 6, a tunneling interface state appears at 1.88 GHz, where the resonant condition $\varphi_1(\omega) + \varphi_2(\omega) = 0$ is satisfied. The measured results are in accordance with the simulated ones except that some attenuations (about 5 ~10 dB) and deviations exist due to the difference between the ideal and real lumped element components. These results verify that the tunneling interface states in SNG pair structures can be understood using the simple resonant condition.

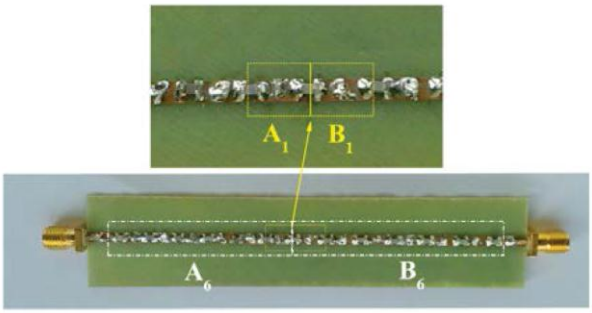

Fig. 5. Photograph of the pair structures A_6B_6 fabricated based on CRLH TLs.

#188556 - $15.00 USD Received 10 Apr 2013; revised 7 Jun 2013; accepted 1 Jul 2013; published 5 Jul 2013

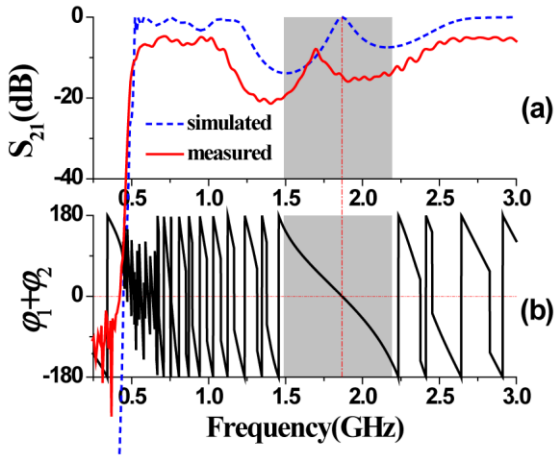

Fig. 6. (a) The simulated and measured *S* parameters and (b) the simulated reflection phase changes $\varphi_1(\omega) + \varphi_2(\omega)$ as a function of frequency for structure A_6B_6. The grey areas represent the common SNG frequency region of TLs *A* and *B*.

3.3 Experiments and simulations on SNG sandwich system

Then, experiments were carried out to study the interface states in SNG sandwich layered structures in the microwave region. Four structures $A_6B_2A_6$, $A_6B_4A_6$, $A_6B_6A_6$ and $A_6B_{12}A_6$ were fabricated based on the CRLH TLs, as shown in Fig. 7. The simulated and measured *S* parameters, together with the sum of the reflection phase changes $\varphi_1(\omega) + \varphi_2(\omega)$ for different structures, are shown in Fig. 8. As shown by the simulation results in Figs. 8(a) and 8(b), two tunneling interface states appear in structure $A_6B_2A_6$ at 1.59 GHz and 2.19 GHz, respectively. As the length of MNG layer increases from B_2 to B_4 then to B_6, the two interface states inside the sandwich structures become closer and closer, and finally merge into each other at frequency 1.88 GHz when the unit number of TL *B* equals 12, as shown in Fig. 8. The experiment results agreed well with the simulations. It is also noted that, within the common SNG frequency region, the sum of the reflection phase changes $\varphi_1(\omega) + \varphi_2(\omega) = 0$ as long as the interface states appear. Such results are in good accordance with the simulations in section 2.3. Therefore, the resonant condition can also be used to predict where the tunneling interface states occur in SNG sandwich structures.

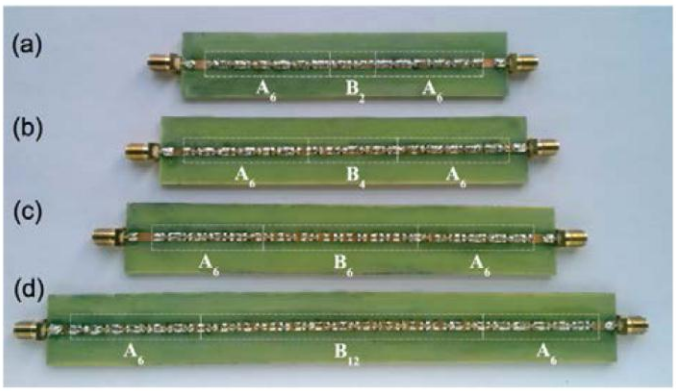

Fig. 7. Photograph of the sandwich structures (a) $A_6B_2A_6$, (b) $A_6B_4A_6$, (c) $A_6B_6A_6$ and (d) $A_6B_{12}A_6$ fabricated using the CRLH TLs, respectively.

#188556 - $15.00 USD Received 10 Apr 2013; revised 7 Jun 2013; accepted 1 Jul 2013; published 5 Jul 2013

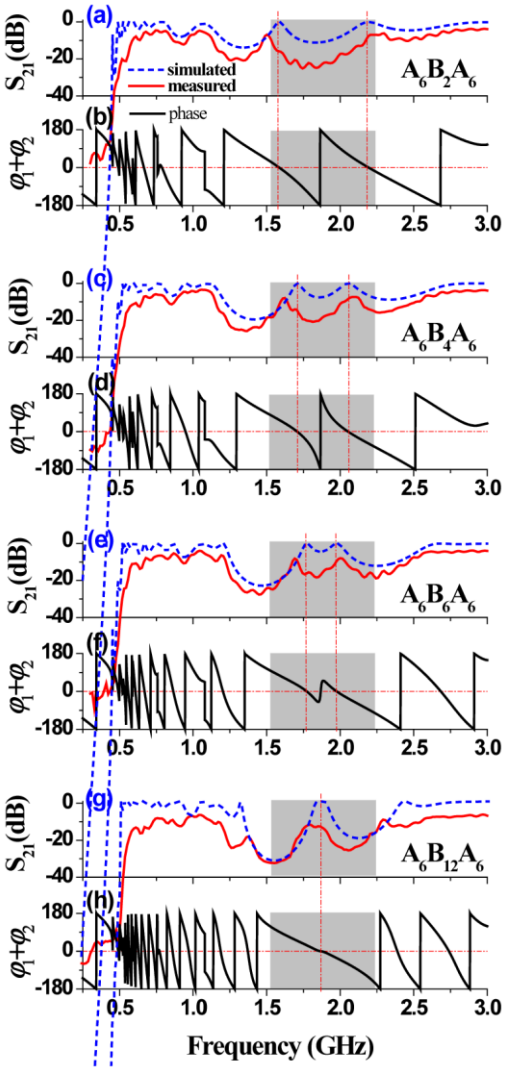

Fig. 8. The simulated and measured S_{21} parameters and the simulated values of $\varphi_1(\omega) + \varphi_2(\omega)$ for SNG sandwich structures $A_6B_2A_6$ (a & b), $A_6B_4A_6$ (c & d), $A_6B_6A_6$ (e & f) and $A_6B_{12}A_6$ (g & h), respectively. The grey regions correspond to the common SNG frequency range of TLs *A* and *B*.

4. Conclusion

In this paper, tunneling interface states in layered structures composed of SNG metamaterials were theoretically and experimentally investigated using a resonant cavity model. The tunneling interface states appeared when the resonant condition, depending on the phase changes inside the resonant cavity, is satisfied. Such a resonant condition is effective for the interface states with perfect or imperfect tunneling transmission. Based on such results, we obtained an effective method to understand and predict where the interface states emerges in the SNG layers through the properties of the phase changes. Both simulations and experimental measurements for SNG layered structure designs confirmed our theoretical expectation. Our research will be useful for designing metamaterial devices with specific interface states that may lead to unusual features, such as resonance, complete tunneling and transparency.

#188556 - $15.00 USD Received 10 Apr 2013; revised 7 Jun 2013; accepted 1 Jul 2013; published 5 Jul 2013

Acknowledgments

This work is supported by National Natural Science Foundation of China (Grant No. 11274126), the Natural Science Foundation of Guangdong Province of China (Grant No. 9151063101000040), and the Hong Kong Polytechnic University (Projects A-PM21, 1-ZV5K, 1-ZV8T, J-BB9P & J-BB9Q). This work is also partly supported by the U.S. Department of Energy (Basic Energy Science, Division of Materials Science and Engineering) under Contract No. DE-AC02-07CH11358.

#188556 - $15.00 USD Received 10 Apr 2013; revised 7 Jun 2013; accepted 1 Jul 2013; published 5 Jul 2013